Preprint
UCRL-JC-145756

ALE3D Model Predications and Materials Characterization for the Cookoff Response of PBXN-109

M. A. McClelland, J. L. Maienschein, A. L. Nichols, J. F. Wardell, A. I. Atwood, P. O. Curran

This article was submitted to
Joint Army Navy NASA Air Force 38th Combustions Subcommittee, 26th Airbreathing Propulsion Subcommittee, 20th Propulsion Systems Hazards Subcommittee and 2nd Modeling and Simulation Subcommittee Joint Meeting, Destin, FL, April 8-12, 2002

March 19, 2002

This work was performed under the auspices of the United States Department of Energy by the University of California, Lawrence Livermore National Laboratory under contract No. W-7405-Eng-48.

ALE3D Model Predictions and Materials Characterization for the Cookoff Response of PBXN-109 *

M. A. McClelland, J. L. Maienschein, A. L. Nichols, and J. F. Wardell
Lawrence Livermore National Laboratory

A. I. Atwood and P. O. Curran
Naval Air Warfare Center – China Lake

ABSTRACT

ALE3D simulations are presented for the thermal explosion of PBXN-109 (RDX, Al, HTPB, DOA) in support of an effort by the U. S. Navy and Department of Energy (DOE) to validate computational models. The U. S. Navy is performing benchmark tests for the slow cookoff of PBXN-109 in a sealed tube. Candidate models are being tested using the ALE3D code, which can simulate the coupled thermal, mechanical, and chemical behavior during heating, ignition, and explosion. The strength behavior of the solid constituents is represented by a Steinberg-Guinan model while polynomial and gamma-law expressions are used for the Equation Of State (EOS) for the solid and gas species, respectively. A void model is employed to represent the air in gaps. ALE3D model parameters are specified using measurements of thermal and mechanical properties including thermal expansion, heat capacity, shear modulus, and bulk modulus. A standard three-step chemical kinetics model is used during the thermal ramp, and a pressure-dependent burn front model is employed during the rapid expansion. Parameters for the three-step kinetics model are specified using measurements of the One-Dimensional-Time-to-Explosion (ODTX), while measurements for burn rate of pristine and thermally damaged material are employed to determine parameters in the burn front model. Results are given for calculations in which heating, ignition, and explosion are modeled in a single simulation. We compare model results to measurements for the cookoff temperature and tube wall strain.

INTRODUCTION

Computational tools are being developed to predict the response of Navy ordnance to abnormal thermal (cookoff) events. The Naval Air Warfare Center[1] (NAWC) and Naval Surface Warfare Center (NSWC) are performing cookoff experiments to help validate DOE computer codes and associated thermal, chemical, and mechanical models. Initial work at the NAWC focused on the cookoff of an aluminized, RDX-based explosive, PBXN-109 that is initially confined in a tube with sealed ends (see Figure 1). The tube is slowly heated until ignition occurs. The response is characterized using thermocouples, strain gauges, and high-speed cameras. A modified version of this system is being developed at the NSWC. The designs of these cookoff systems are relatively simple to facilitate initial model development. An effort is being made to achieve a wide range of results for reaction violence.

Lawrence Livermore National Laboratories (LLNL) and Sandia National Laboratories (SNL) are developing computer codes and materials models to simulate cookoff for ordnance safety evaluations. The computer program ALE3D from LLNL is being used to simulate the coupled thermal transport, chemical reactions, and mechanical response during heating and explosion[2]. SNL is employing multiple computer codes in a parallel effort[3,4,5]. For the analysis of PBXN-109 cookoff, Schmitt et al.[6] performed an initial survey of measured materials properties and provided estimates for several others. In addition, they performed initial predictions of the time to explosion for a small-scale NSWC cookoff system. Atwood et al.[7] measured mechanical, physical, and chemical properties of PBXN-109. Erikson et al.[8] performed thermal, chemical, and mechanical simulations of the NAWC tests. Their predicted cookoff temperatures are generally in good agreement to values measured in several NAWC tests[1]. They also

---

* Approved for public release, distribution is unlimited. Work performed under the auspices of the U.S. Department of Energy by Lawrence Livermore National Laboratory under contract No. W-7405-ENG-48.

presented initial calculations showing the expansion of the containment tube after ignition. In an earlier paper[9] we discussed ALE3D models for cookoff of PBXN-109 in the NAWC system of Figure 1, and presented measurements for thermal expansion, heat capacity, shear modulus, bulk modulus, and ODTX. Later those measurements were used to determine model parameters, and ALE3D predictions for explosion temperature were in satisfactory agreement with NAWC measurements[10, 11]. He we present initial ALE3D simulations for slow cookoff in which thermal, mechanical, and chemical behavior is modeled through the heating, ignition, and explosion phases. Results are compared for explosion temperature and tube wall strain.

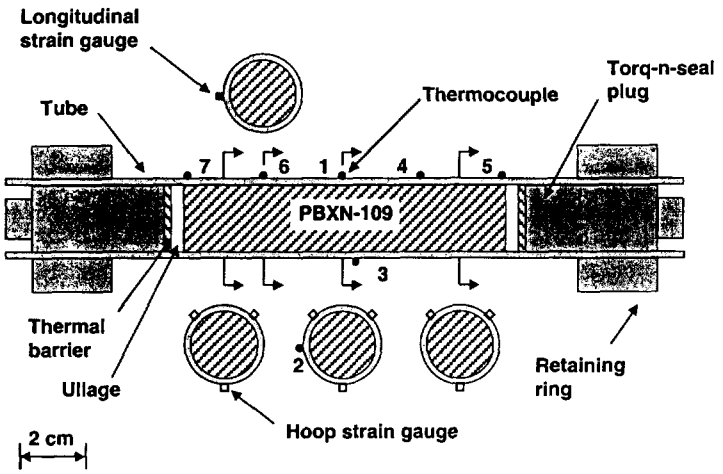

Figure 1 Schematic of geometry and instrumentation for NAWC cookoff tests.

MODEL VALIDATION EXPERIMENTS

The NAWC is performing cookoff tests with cylindrical charges of PBXN-109 confined in a steel tube with sealed ends[1] (see Figure 1). The explosive has a nominal aspect ratio of L/D=4, and a diameter nearly matching the inside diameter of the tube. For a representative test (No. 000819) the 4130 steel tube has a 2.52 cm outer diameter with a 0.21 cm wall thickness providing a confinement pressure of approximately 0.7 kbar (70 MPa). The end seals are achieved with torque-n-seal plugs secured with retaining rings. Ullage is adjusted at the ends of the energetic material by changing the axial positions of the end plugs. Insulating materials are placed at the ends of the explosive and tube. An insulated wire wrap provides the energy to heat the tube. The assembly is mounted horizontally in a vise and enclosed in a sealed box.

For Test No. 000819, the temperature is measured at seven locations on the outer tube surface using thermocouples. A Proportional-Integral-Derivative controller is used to adjust the heater power to keep the center-top temperature, TC1, near the set-point value. Nine hoop strain gauges and one longitudinal strain gauge are used to measure the deformation of the tube during thermal ramp and explosion. A high-speed camera is available to monitor the expansion and fragmentation of the assembly. In this experiment, the final ramp rate for the set-point temperature was 6°C/h.

ALE3D MODEL

ALE3D chemical, mechanical, and thermal models are being developed to model the cookoff of PBXN-109. In our initial model, the chemical reaction sequence is taken to have four components with three reaction steps following the model developed by McGuire and Tarver[12] for pure RDX:

$$A \rightarrow B \qquad r_1 = Z_1 \exp(-E_1/RT)\rho_A \tag{1}$$

$$B \rightarrow C \qquad r_2 = Z_2 \exp(-E_2/RT)\rho_B \tag{2}$$

$$C \rightarrow D \qquad r_3 = Z_3 \exp(-E_3/RT)\rho_C^2 \tag{3}$$

Here ρ_i is the mass concentration of a reactant i. The quantities r_j, Z_j and E_j are the reaction rate, frequency factor and activation energy, respectively, for a reaction j. Component A is the starting material including RDX, aluminum, and binder. Component B is an intermediate with material properties assumed to be the same as component A, and the components C and D are treated as gases. The aluminum particles and binder are treated as inert until the last reaction step where they are converted to their final products. The aluminum particles and binder are treated as inert until the last reaction step where they are converted to their final products. The question can be raised as to the extent that the aluminum burns during the tube expansion. We have selected one limiting case while other investigators[8] have treated the aluminum as unreactive. The selection of parameters and a comparison of model ODTX predictions with measured values are given below.

After the Arrhenius reaction rates have increased to the point where changes are occurring on a time scale approximately 10X the time scale of sound propagation, a switch is made to a burn front model in which reactants are converted to products in a single reaction step. This switch in models is made for two reasons. The first is that the computational capabilities and methods are not yet available to resolve reaction zones which can be on the scale of nanometers. The second reason is that Arrhenius kinetics measured on the time scale of $1\text{-}10^4$ s in the ODTX apparatus may not apply on shorter time scales. It is likely that deflagration rates measured in the strand burner described below provide a better measure of reaction behavior on short time scales. We assume that the burn front velocity, V, is a function of the pressure, P, at the front location, and use a power-law expression of the form:

$$V = V_0(p/p_0)^n \tag{4}$$

Here the subscript 0 indicates a reference quantity. The selection of parameters for PBXN-109 is discussed below in the section on burn rates.

The mechanical models for the chemical constituents A and B along with the steel components are taken to have Steinberg-Guinan[13] strength models. For PBXN-109, the model expressions for shear modulus and yield stress are taken to be

$$G = G_0 - b(T - T_0) \qquad Y = Y_0 G/G_0 \tag{5}$$

In which the subscript "0" denotes values at room temperature (20°C). The parameters G_0 and b are estimated from oscillatory shear modulus measurements as described below. A polynomial expression is used for the equations of state:

$$p = p_0 + K_0\mu + a_1\mu^2 + a_2\mu^3 + (\gamma_0+\gamma_1\mu)\rho_0 c_v(T-T_0) \tag{6}$$

in which

$$\mu = \rho/\rho_0 - 1 \tag{7}$$

Note that additional terms for strain hardening appear in Eq. (5) for steel[13]. The constant volume heat capacity c_v does not vary with temperature. Calculated melt and cold curves are used to account for the influence of compression on melting energy. In previous studies[10, 11], a nonlinear regression procedure was used to determine the coefficients K_0, a, and γ_0 that give an optimum representation of the measurements of CTE, hydrostatic compression, and the unreacted shock Hugoniot described below (see Table 1). Comparisons between model and experimental values show that the Steinberg-Guinan models provide only an approximate description of the measurements. The Steinberg-Guinan models were developed for metals, and PBXN-109 is a complex composite material consisting of relatively brittle

RDX, rubber-like binder, and loosely bound aluminum particles. In addition, the Steinberg-Guinan model for 4340 steel is used for the 4130 steel. The influence of these approximations is a subject of continuing investigation.

Table 1 Selected Parameters for Strength and EOS Models

Material parameter	Units	PBXN-109 Solid Species A, B	PBXN-109 Gas Species C, D	4130 steel[10]
K_0	GPa	2.82		159
a_1	GPa	17.3		160
a_2	GPa	144.0		0
γ_0		0.461		1.65
γ_1		0.461		0.5
G_0	GPa	4.68×10^{-3}		77.0
B	GPa/°C	1.10×10^{-5}		5.05×10^{-2}
Y_0	GPa	0.06		1.03
ρ_0	g/cm^3	1.67		7.83
c_v	J/g-°C	1.33	1.96	0.444
λ	W/m-°C			
20°C, 1 bar				42.7
90°C, 1 bar		0.454		
400°C, 1 kbar			7.89×10^{-2}	
2000°C, 1 kbar			7.28×10^{-2}	
Γ			1.163	

The model chemical components C and D are treated as no-strength materials with gamma-law equations of state:

$$p = (\Gamma - 1)\, \rho c_v T \qquad (8)$$

This equation of state is appropriate for the relatively low confinement pressures (~1 kbar) of these cookoff tests. The Γ-value for species C and D is set using a pressure of 1 kbar, a temperature of 2273°K, and the density and heat capacity c_v from the thermo-chemical equilibrium computer code, CHEETAH 2.0[14] for the final product gases (see Table 1).

The time-dependent thermal transport model includes the effects of conduction, reaction, advection, and compression. The constant-volume heat capacity is constant for each reactant consistent with the Steinberg-Guinan model. The thermal conductivity for the solid species A and B is taken to be constant, whereas the effects of temperature are included for the gaseous species. The thermal properties for materials A and B are listed in Table 1 and are assigned using the measurements of this project for PBXN-109 as described in earlier studies[10, 11]. The heat capacity c_v for gases C and D is assigned the same constant-volume value used in the gamma-law model. The temperature-dependent thermal conductivity is estimated at 1 kbar using Bridgman's[15] equation for liquids in which the sound velocity is calculated using results from CHEETAH (see Table 1).

CHEMICAL KINETICS MEASUREMENTS AND MODEL REPRESENTATION

Here we report on our measurements and ALE3D model representations of one-dimensional-time to explosion and burn rate for PBXN-109. The PBXN-109 mixture has a nominal composition of 64% RDX, 20% Al, and 16% HTPB/DOA binder by weight[7]. The samples were taken from mixture no. 991206 that is being used by the participants from LLNL, SNL, NAWC, and NSWC in this cookoff investigation.

One-Dimensional-Time-to-Explosion (ODTX)

ODTX measurements were made for PBXN-109 using the standard apparatus at LLNL[16]. In this system, the outer surface temperature of a 1.27 cm diameter sphere of HE is suddenly increased to a higher set-point temperature. The time to explosion is the time elapsed from the start of heating until

confinement failure. The measurements of this study along with previous measurements are plotted as a function of temperature in Figure 2. The present measurements include results with and without a leak channel (unconfined). Both sets of results follow a single curve suggesting the insensitivity of explosion time to pressure. The present measurements are consistent with the earlier PBXN-109 results except at explosion times below 10 sec where the measurement limits of the apparatus are being approached.

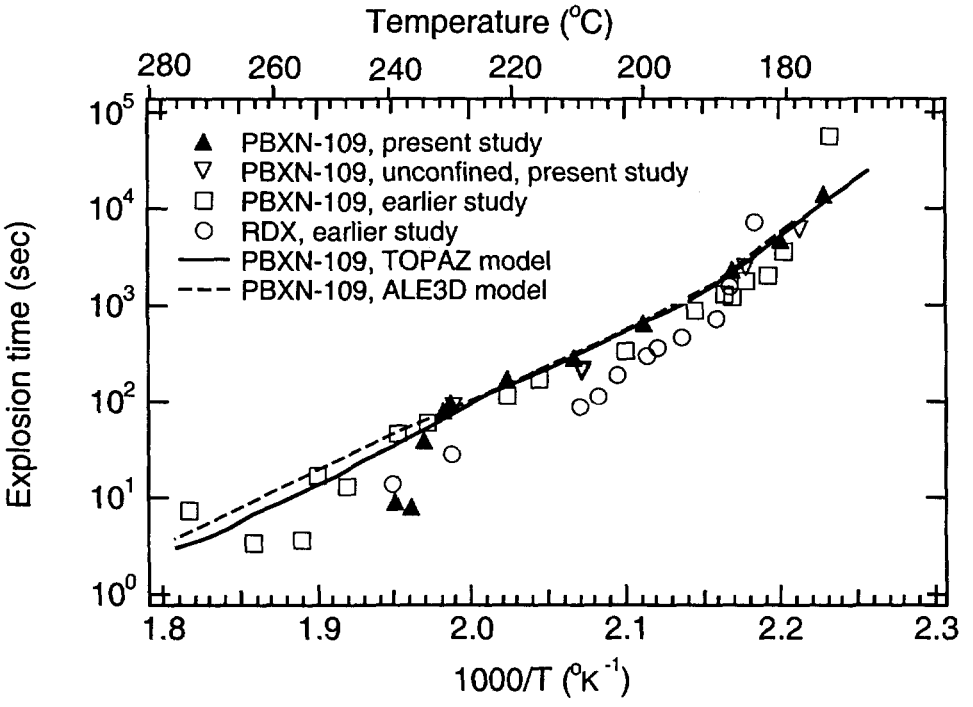

Figure 2 Comparison of ODTX results for PBXN-109 and RDX.

Calculated explosion times for PBXN-109 are also shown in Figure 2 for a one-dimensional model involving transient heat conduction and the chemical reaction sequence[12] (Eqs. (1)-(3). In this model, the densities of each of the four components A, B, C, and D are taken to have the room temperature value of 1.67 g/cm^3. The two components A and B are assumed to have the same thermal transport properties. We use the heat capacities and thermal conductivities of Table 1. The values of E_j in Table 2 are the same as those of McGuire and Tarver [12]. The values of $\ln(Z_j)$ are shifted by a single offset value as described below to provide an optimal fit of the confined measured explosion times. A model to satisfactorily represent all of the measurements has not yet been completed. The two highest temperature points were not included in the regression procedure in order to provide a better fit of the lower temperature data that is most relevant to slow cookoff. The RDX heats of reaction q_1 and q_2 for the first two steps are reduced by 36% to account for the fraction of RDX present in the mixture. The aluminum and the binder are treated as inert until the final reaction step. The value for q_3 is calculated using q_1 and q_2 and the total heat of reaction of 1696 cal/g calculated from CHEETAH[14]. One-dimensional explosion times were calculated using TOPAZ2D[17, 18] and a mesh with 50 elements uniformly spaced in the radial direction. The time to explosion is taken to occur at the time that 10% of the initial mass of HE is converted to the final product D[18]. A nonlinear regression procedure incorporating the Davidon-Fletcher-Powell method[19] was used to adjust the single shift in $\ln(Z_j)$ to provide the best fit of the measured values by the TOPAZ2D values. The resulting model explosion times match the measured values over much of the temperature range (see Figure 2). However, there are larger discrepancies between the model values and the measurements of this study at temperatures above 235°C. It is also of interest to note that in this same temperature range measurements of the current study differ significantly from the results of the earlier study which exhibit considerable scatter. Nonetheless, the model is expected to provide satisfactory results at the lower temperatures observed at ignition in the cookoff tests.

Table 2 Chemical Kinetics Parameters for PBXN-109

Reaction step	$\ln(Z_j)$	E_j kcal/g-mole-°K (kJ/g-mole-°K)	q_j cal/g (J/g)
A→B	43.7 s^{-1}	47.1 (197)	64 (268) endothermic
B→C	38.9 s^{-1}	44.1 (185)	-192 (-803) exothermic
C→D	32.7 s^{-1}-cm^3- g^{-1}	34.1 (143)	-1568 (-6560) exothermic

Also shown in Figure 2 are results for the ALE3D code for the case of reaction and thermal transport without material motion. We use the same parameters of Tables 1 and 2 employed with TOPAZ2D. Additional details are given below on the solution strategy. We used a 1D spherically symmetric mesh that also has 50 uniform elements. The results agree within 2% for temperatures below 235 °C, but variations of the scale 10% are seen for higher temperatures. This discrepancy is attributed to incomplete resolution of the conduction boundary layer at short times which is less important in slow cookoff cases.

Burn Rate Measurements for PBXN-109

The deflagration rate of pristine and thermally-damaged PBXN-109 was measured with the LLNL High Pressure Strand Burner. This system measures pressure during the burn and also the progress of the burn front with wires that melt as the flame approaches. Cylindrical samples 6.4 mm diameter x 5.7 cm long are prepared by stacking nine pieces to form a burn tower. Temporal pressure data along with time of arrival data at each burn wire provide the information to calculate burn rate as a function of pressure. Further details have been given by Maienschein et al.[20-22].

Results from deflagration rate measurements with pristine PBXN-109 are shown in Figure 3. The deflagration behavior of PBXN-109 is remarkably stable over the entire pressure range, with data showing smooth and consistent increases with pressure within each run and from run to run. Also shown in Figure 3 are data at the lower end of our pressure range measured at NAWC[23]. The LLNL and NAWC results show excellent agreement.

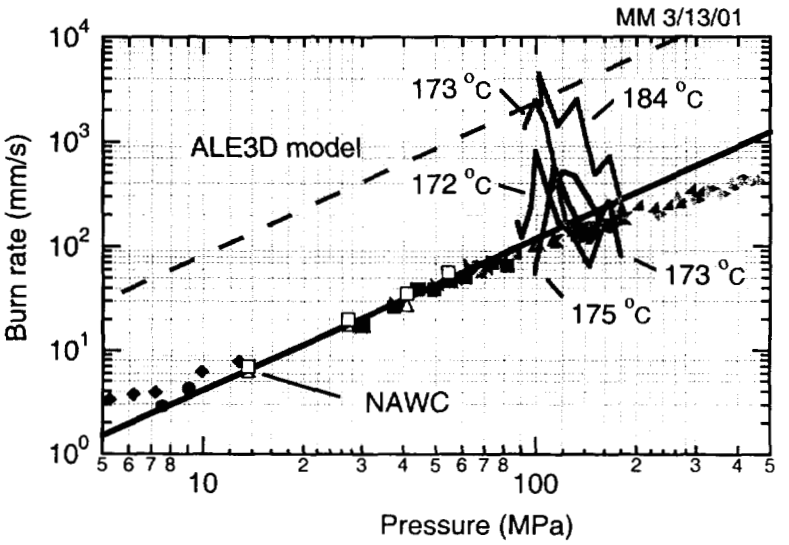

Figure 3. Deflagration rate data for pristine and thermally-damaged PBXN-109. Solid symbols represent LLNL measurements. Each set of symbols represents data from one experiment. Open symbols represent data from Atwood[23].

In modeling the NAWC thermal explosion experiments, we need the deflagration behavior of the PBXN-109 after it has been heated and thermally damaged. Characterizing the damage caused by high

temperatures is difficult. We chose to not attempt such characterization at this time, but instead chose to thermally damage the PBXN-109 using time-temperature treatments matching those in the NAWC cookoff tests. Therefore, the deflagration behavior measured with these samples should directly reflect the expected deflagration behavior of the PBXN-109 during the actual thermal explosions. We note that this approach does not provide sufficient information to allow general prediction of the effect of thermal damage on deflagration; nonetheless, it does provide data sufficient to support the modeling of the specific NAWC tests.

The NAWC experiments were run with heating rates of 3 and 6°C/hr. We heated samples at these heating rates to a specified temperature after an initial heating to 130°C followed by a thermal soak for ~ 45 minutes to allow thermal equilibration. Then the deflagration was initiated if the sample had not already self-ignited. The deflagration rate data as measured by the burn wires is shown with ignition temperatures in Figure 3.

The data in Figure 3 show an increase in deflagration rates of up to 10-20 fold for thermally damaged samples. All samples showed this very fast deflagration for about the first third of the sample, with the remainder of the sample burning at rates about the same as or slightly slower than the pristine material. We do not have an explanation of this behavior, but it quite reproducible. An analysis of vivacity[24] (dlnP/dt) suggests that the initial surface area of the thermally-damaged material is as much as a factor of 20 larger than for the pristine material. This result appears to be consistent with the burn velocity measurements.

For the application of ALE3D, we use the following parameters for the burn-rate expression (4)

$$V_0 = 1.00\text{x}10^{-1}\ \text{mm/s} \qquad P_0 = 0.1\ \text{MPa} \qquad n = 1.46$$

Here n is the value obtained by Atwood et al.[23] which represents the pressure dependence of their measurements and those obtained at LLNL in the lower portion of the pressure range. The coefficient V_0 is a factor of 20 larger than the value for the pristine-material value to represent the increase in velocity resulting from damage during the long thermal ramp. This model will be refined based on additional measurements for thermally-damaged materials.

BOUNDARY CONDITIONS AND NUMERICAL METHOD

Boundary Conditions

A two-dimensional , axisymmetric ALE3D model is used to simulate the cookoff of PBXN-109 in cookoff Test No. 000819. Boundary conditions for this model are shown schematically in Figure 4. Although the full length of the domain is shown, a plane of symmetry was employed half way between the two ends. The two-dimensional model includes 10% ullage on the HE ends and no ullage on the side. The gaps are filled with a void material described above that has the thermal transport properties of air. The HE does not slip at the wall, and the plug and retaining ring are taken to be joined to the tube wall. The ends of the tube and plug at the spacer block are treated as free mechanical boundaries in which energy losses are handled with a heat transfer coefficient. The tube heater is modeled as a uniform thermal flux condition at the outside tube surface between the retaining rings. The heat flux is adjusted using a PI controller to maintain TC1, the top-center tube temperature, at its set-point value (see Figures 1 and 4). The PI controller is tuned using the strategy of Internal Model Control[25] in which the steel tube wall is treated as a first-order lumped-capacitance system with a single heat transfer coefficient to account for thermal losses to the surrounding air. Thermal convection is applied to all outward facing surfaces using heat transfer coefficients for laminar flow of air past a horizontal cylinder[26]. Standard expressions for hemispherical radiation are used on these same surfaces. Heat transfer coefficients are reduced on the outside surface of the heater to account for the influence of insulation.

Since there are large uncertainties concerning contact resistances between the plug, tube, and vise, adjustments are made in the heat fluxes at the outside surface of the ring. A model PI controller is added to adjust the uniform heat flux at these surfaces to match linear representations of the measured temperatures at the end thermocouples TC5 and TC7. Each end thermocouple trace is fit by the expression

$$T = T_\infty + c(T_{set} - T_\infty) \qquad (9)$$

in which c is the fit parameter, T_{set} is the set-point temperature for TC1, and T_∞=20°C is the ambient temperature. The resulting values for c associated with TC5 and TC7 are averaged and used as a set point for the additional model controller. This approach allows the thermal conditions to be easily and accurately represented for evaluation of the HE response.

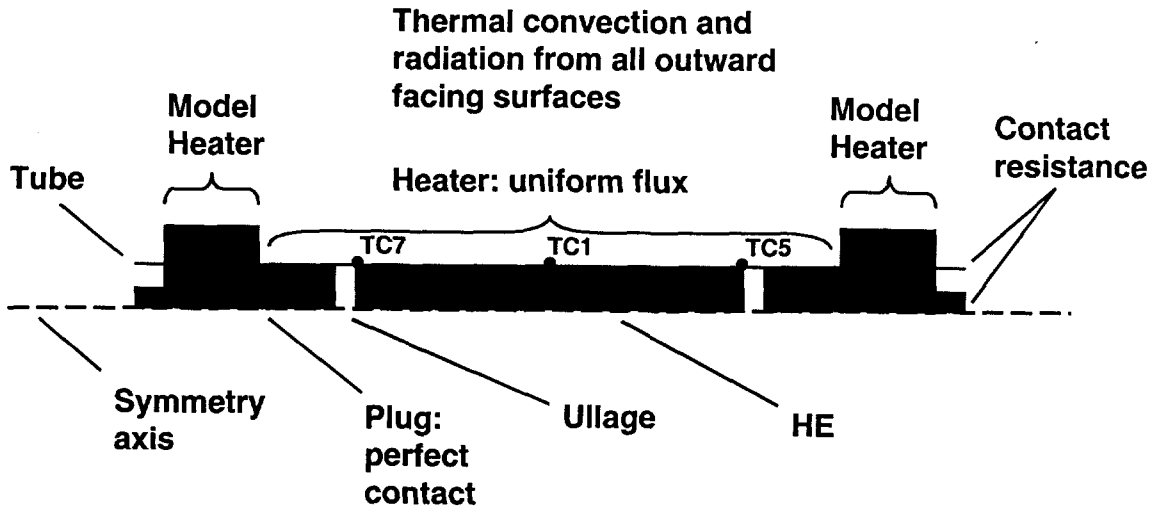

Figure 4 Boundary conditions for ALE3D axisymmetric model of NAWC cookoff. In this study a symmetry plane is employed at TC1.

Meshes and Numerical Strategy

The ALE3D computer code requires 3D meshes, and a wedge-shaped mesh is employed for the 2D model of this study (see Figure 5). A small hole is present near the symmetry axis to allow the use of hexahedral elements at all locations. The tube cavity has 12 elements in the radial direction, 20 in the axial direction, and 1 element in the azimuthal direction. Initially, the HE occupies the entire cavity in the radial direction and 90% of the cavity in the axial direction (see Figure 5). The remainder of the tube cavity is filled with air modeled as the void material discussed above. Some of the elements have both HE and air, and standard mixing rules are employed to calculate the energy, heat capacity, thermal conductivity, shear modulus, and equation of state[27]. Since PBXN-109 is a soft material that undergoes large deformation while expanding in the cavity, the mesh is smoothed using a combination of Lagrange and Eulerian algorithms. Nodes initially on the interface between the cavity and the steel remain on these boundaries while nodes interior to the cavity are advected through the flowing HE and air.

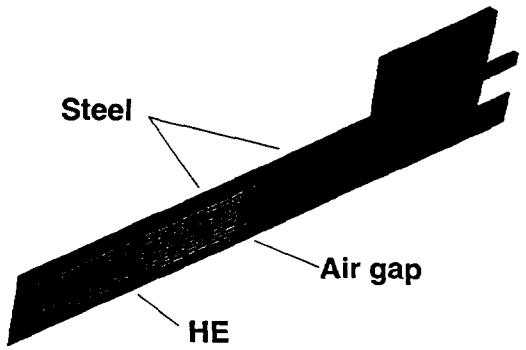

Figure 5 ALE3D axisymmetric wedge mesh for cookoff of PBXN-109 in NAWC Test 000819

A fully implicit method is used for the integration of the thermal transport equations during the the thermal ramp and much of the subsequent ignition process. After the time step has decreased to within a factor of 10 of the value given by the Courant condition, a switch is made from implicit to explicit integration of the thermal transport equation. During the thermal ramp and subsequent ignition process, the hydrodynamic equations are integrated using an explicit method with the material densities increased by a large scale factor to make the calculation computationally feasible. Otherwise the time step size would be a fraction of a microsecond in a cookoff test lasting 9 hours. During the ignition process, this scale factor for the density is reduced in steps as the time-step size decreases to track the accelerating chemical reactions. Eventually the scale factor becomes unity and all equations are integrated explicitly with the densities at their physical values. There are two major benefits of using an explicit hydrodynamic integration method . The explicit numerical scheme can accommodate the very soft PBXN-109 which is not readily handled with the current ALE3D implicit scheme for hydrodynamics. In addition, current algorithms for slide surfaces are compatible with explicit schemes. Although results for slide surfaces are not presented in this study, work is in progress with this method since it provides mesh tracking of the HE boundaries within the cavity, giving a more accurate solution.

After a zonal temperature reaches a user-specified threshold value, the multi-step kinetics model is replaced by the burn front expression (4). The burn front is propagated through the PBXN-109 with the assumption that reactants are converted completely to products in a single step. This burn front is tracked using a level set method that conserves mass, momentum, and energy across the front. Since the mesh is not moved to explicitly track the front, the resolution of the burn front is on the scale of the mesh element size. The effects of mesh size are an important consideration under current investigation.

COMPARISON OF MODEL AND MEASURED THERMAL COOKOFF RESULTS

In cookoff Test 000819 for PBXN-109, the set-point temperature for TC1 was increased at 600°C/h from room temperature to 130°C, held for 0.5 h, and then increased at 6°C/h until cookoff[1] (see Figures 1 and 6). The measured thermocouple temperature, TC1, tracks the set point with some noticeable fluctuations (±1°C) until cookoff at a set-point temperature of 174°C. The end thermocouples TC7 and TC5 give very similar temperature profiles, indicating symmetry about the axial mid-plane which is an assumption of this numerical analysis. The temperatures of TC5 and TC7 are 10 to 14 °C less than TC1 which indicates significant cooling at the tube ends. Thus, large temperature gradients are present along the length of the HE, creating a well-defined hot zone near the axial mid-plane.

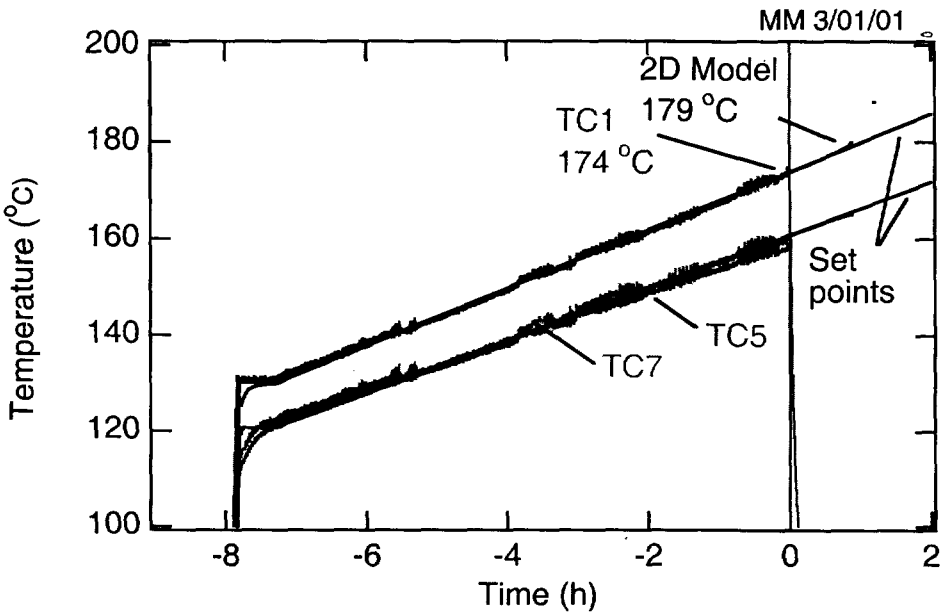

Figure 6 Comparison of measured and model tube wall temperatures for NAWC-CL Test No. 000819.

The model controller tracks the TC1 set point well through both the fast and slow ramps (see Figure 6). Note that the controller gain was reduced by a factor of two after the initial steep ramp to increase numerical efficiency during periods of slow change in the set point. The TC5 and TC7 traces were fit according to the procedure described above, and an average trace was used as a set point in an auxillary model controller providing heat at the outside surface of the retaining ring. The model controller keeps the calculated temperature at the end of the HE near the measured values for TC5 and TC7.

The cookoff temperature for the 2D model is 179.0°C which is somewhat larger than the measured value of 174°C. Note that the cookoff temperature is taken to be the value of the set-point temperature for TC1 at the time of cookoff. In order to help determine the source of this difference, we make use of a 1D axisymmetric model studied earlier[10] to evaluate the impact of cooling at the ends which is zero for the 1D case. The 1D model with no axial gradients gave a cookoff temperature 2 °C less than the 2D model with a ~20 °C temperature drop from center to end. This result suggests a minimal influence of uncertainties relating to cooling at the tube ends. The 1D model was also used to examine the possible effects of mesh refinement. The number of zones in the radial direction was increased from 12 to 96 with no significant change (<1%) in the cookoff temperature. This suggests that the 2D results are sufficiently resolved in space for time-to-event calculations. It is believed that the 5°C discrepancy between measured and model cookoff temperature has its source in the chemical kinetics model.

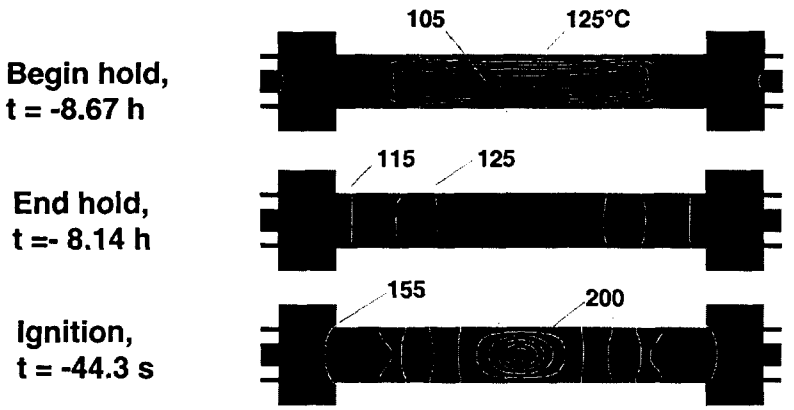

Figure 7 Temperature contours for ALE3D axisymmetric model for NAWC-CL Test No. 000819. Contours increase from 100 °C to 200°C in 5°C increments.

Two-dimensional temperature fields are shown in Figure 7 after the initial steep ramp, after the hold, and prior to cookoff. Strong radial temperature and axial temperature gradients are observed after the steep ramp at the beginning of the hold period. At the end of the hold period, the primary variations are in the axial direction as desired. The predicted ignition location is near the axis of symmetry and axial midplane. This result is confirmed by tube fragments which show failure in the middle of the tube (see Figure 8).

Calculated density fields show the filling of the air gaps, the formation of HE product gases, and the expansion of the tube wall in NAWC Test No. 000819 (see Figure 9). At t=5.4 μs, product gas is forming at the center of the HE, and the expanding HE is filling the void areas at the ends of the cavity. At t=53 μs, the expanding HE has filled all but a small region at the corner of the tube cavity, and HE product gases occupy a large region at the center of the HE. At t=320 μs, the ullage has disappeared, product gases are present across the entire diameter of the tube cavity, and the tube wall has extensively expanded and thinned. At this time it is likely that the tube wall would have ruptured and fragmented.

The model strain curve is compared with measurements for three surface strain gauges at the axial mid-plane (see Figures 1 and 10a). These three hoop strain guages are spaced at 120 degrees along the outside of the tube and provide measurements with a limit of approximately 1.5% strain[1]. These gauges provide measurements of the total strain which includes the contribution of the steel tube. Strain gauge signals are zeroed at the ambient temperature. Strain gauges SG4 and SG6 give very similar

results, but some there is some lag for SG5. These results suggest a fairly symmetrical initial expansion of the tube.

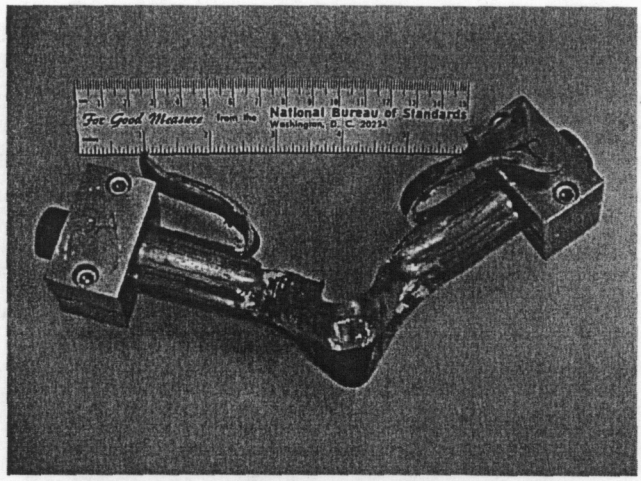

Figure 8 Tube fragments from NAWC-CL Test No. 000819.

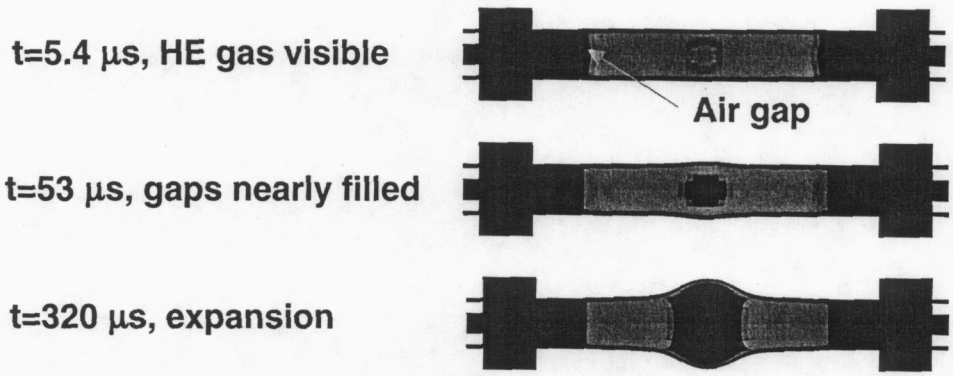

Figure 9 ALE3D density fields for axisymmetric ALE3D model of NAWC-CL Test No. 000819.

The ALE3D model does not yet provide a good representation of the measurements. The model strain initially decreases slowly from 0.6% at t=- 20 μs and then more rapidly to 0.3% at t=19 μs before increasing at a rate higher than observed in the experiment. (Note that 17.7 μs is added to the model times in Figure 10a for comparison with the measurements.) There are several factors that could contribute to this apparently anomalous feature. The first portion of this decrease at t=17.7 μs occurs at the same time that the switch is made from Arrhenius kinetics to the power-law burn rate model. Another contributing factor may be the use of the very low shear modulus for PBXN-109 giving almost "liquid-like" behavior (see Table 1). This type of model can be difficult to handle numerically. The effects of varying the shear modulus are discussed further below. Another factor could be the use of the mesh smoothing routines (advection) in conjunction with the mixing of gases and solid with greatly differing densities.

The model strain curve at longer times and higher strains shows a period of rapid increase, a plateau, and then a continued increase (see Figure 10b). The pressure buildup associated with the initial burning results in the initial increase in strain. At the same time the soft PBXN-109 is driven rapidly into the air gaps at the end of the tube cavity (see Figure 9). Pressure waves propagate along the axis of the tube. During the strain plateau, strain hardening may be limiting the expansion of the tube at the axial midplane and cause the strain to be distributed over the length of the length of the tube cavity. After the

yield strength is reached at the axial mid-plane, the strain rate increases rapidly. Thus, the model is generating behavior that might be expected for a rapidly pressurized liquid in a sealed tube.

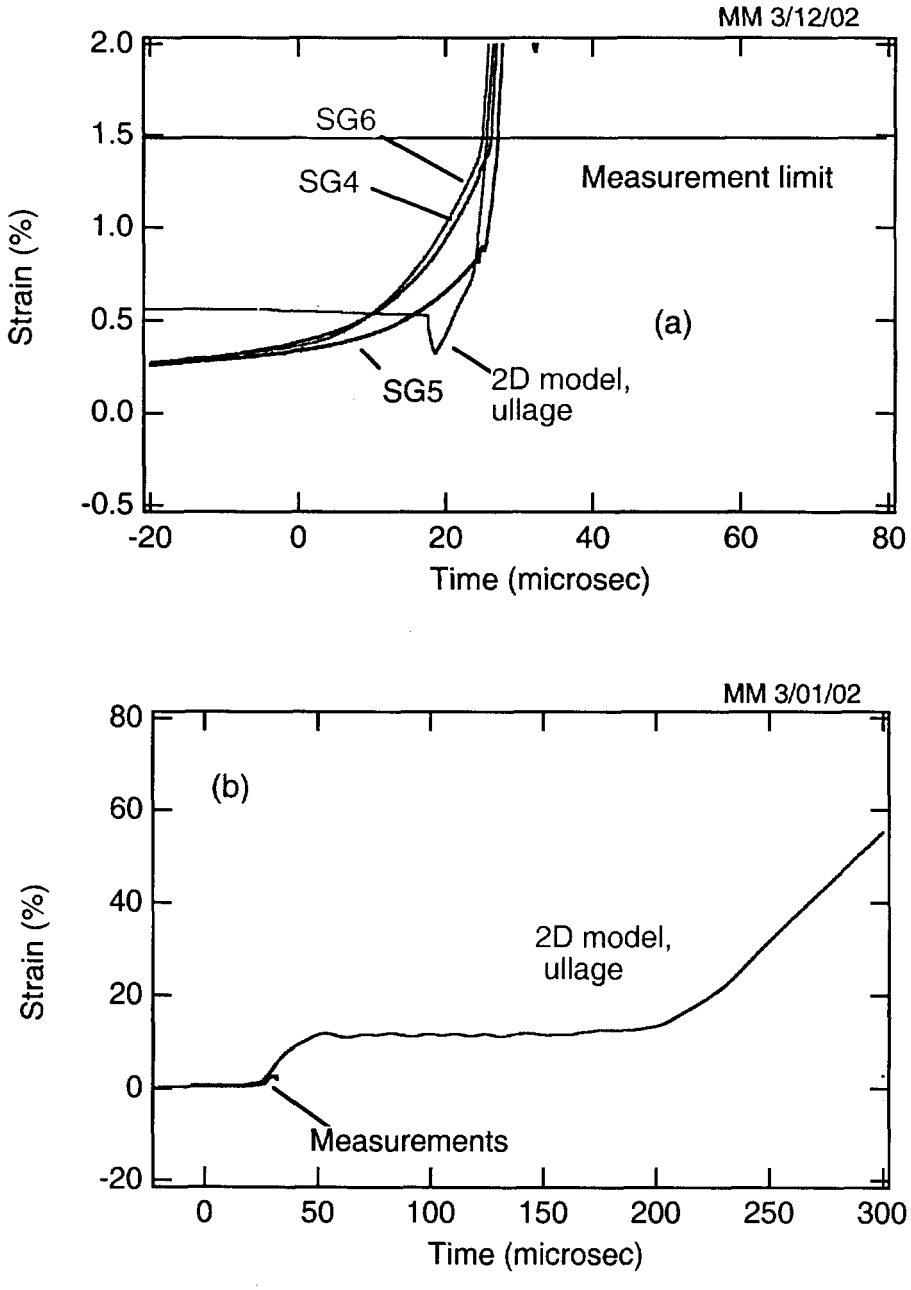

Figure 10 Comparison of ALE3D strains with measurements for NAWC-CL Test No. 000819 on (a) small and (b) large strain scales.

In other simulations not shown here, the pressurization and filling of the cavity ends was greatly reduced with the use of a shear modulus 100X larger than the value of Table 1. The hoop strain at the axial mid-plane grew monotonically without an initial dip or subsequent plateau. Since the properties of the PBXN-109 may vary greatly after a 9-hour temperature ramp, the question remains as to the mechanical properties of the damaged material at the time of ignition. We are continuing to investigate

the influence of shear behavior, transition in kinetics models, and materials mixing models on the model strain curve.

CONCLUSIONS

An NAWC cookoff test is analyzed using the ALE3D computer code which incorporates models for thermal, mechanical, and chemical behavior. In the NAWC cookoff experiments, a PBXN-109 sample with L/D=4 is heated slowly in a sealed tube until explosion. The ALE3D code is used to simulate thermal, mechanical, and chemical behavior on the long time scales of heating and short time scales of explosion. The Tarver-McGuire model was selected to represent the chemical kinetics behavior during heating, and the power-law burn model was employed during the rapid expansion phase. Parameters for the Tarver-McGuire model were specified using ODTX measurements, and power-law parameters were taken from strand burner measurements. Burn rate measurements for thermally-damaged PBXN-109 show dramatically more rapid and irregular burning than for pristine material. A Steinberg-Guinan mechanical model and polynomial EOS is selected for the PBXN-109 solid species. A Gamma-Law model is used for the product gases, and the air in gaps is represented with a "void" model. Parameters for the mechanical and thermal models are specified using earlier measurements of shear modulus, bulk modulus, CTE, unreacted shock Hugoniot, heat capacity, thermal conductivity, and density. Cookoff simulations for a two-dimensional axi-symmetric model were completed for the thermal ramp, ignition, and rapid expansion of the tube. For the test considered, the predicted cookoff temperature is in satisfactory agreement with the measured value. However, the model does not yet provide a good representation of the measured strains. Improvements to the burn model, strength model, and transition from the multi-step kinetics model to a single-step kinetics model are expected to lead to improved predictions.

ACKNOWLEDGMENTS

John Reaugh and Craig Tarver are acknowledged for their valuable input on model development. Brad Wallin helped with the development and use of the ALE3D computer code. Bill Erikson of SNL contributed to the model development.

NOMENCLATURE

A, B, C, D	Components in chemical reaction sequence
a_1, a_2	Parameters in polynomial EOS (Eq. 6)
ALE3D	Chemical-mechanical-thermal code using Abitrary Lagrange Euler meshes in 3D
b	Parameter in Eq. (4), $M/(t^2LT)$
CTE	Coefficient of Thermal Expansion, (1/T)
c_v	Heat capacity at constant volume, (L^2/t^2T)
DOA	DiOctyl Adipate
DOE	Department of Energy
DSC	Differential Scanning Calorimeter
E	Elastic modulus, $M/(t^2L)$
E_j	Energy of activation for reaction j, E/(Tmole)
G	Shear modulus, $M/(t^2L)$
HTPB	Linear Hydroxy-Terminated Polybutadiene
K	Bulk modulus, $M/(t^2L)$
K_0	Bulk modulus in polynomial EOS (Eq. 6), $M/(t^2L)$
n	Reaction order
p	Pressure, $M/(t^2L)$
p_0	Reference pressure, $M/(t^2L)$
NSWC	Naval Surface Warfare Center, Indian Head
ODTX	One-Dimensional Time to Explosion
PBXN-109	Aluminized RDX explosive
RDX	Cyclotrimethylene trinitramine
RMS	Root Mean Square

r_j	Rate of reaction j, $M/(L^3t)$
T	Temperature, T
T_0	Reference temperature, T
TMA	Thermal Mechanical Analyzer
V	Burn front velocity, L/t
V_0	Reference burn front velocity, L/t
Y	Yield stress, $M/(t^2L)$
Z_j	Frequency factor for reaction j, $L^{3(n-1)}/(M^{(n-1)}\ t)$
γ_0, γ_1	Parameters in polynomial EOS (Eq. 6)
λ	Thermal conductivity, E/(tLT)
ρ_i	Mass concentration of reactant i, M/L^3

REFERENCES

1. Atwood, A. I., P. O. Curran, M. W. Decker and T. L. Boggs, "Experiments for Cookoff Model Validation," Proceedings of JANNAF 37th Combustion and 19th Propulsion Systems Hazards Subcommittee Meetings, Monterey, CA, CPIA, 2000.

2. Nichols, A. L., R. Couch, R. C. McCallen, I. Otero and R. Sharp, "Modeling Thermally-Driven Energetic Responses of High Explosives," Proceedings of 11th International Detonation Symposium, Snowmas, CO, Office of Naval Research, 1998.

3. Gartling, D. K., R. E. Hogan and M. W. Glass, "Coyote – A Finite Element Code for Nonlinear Heat Conduction Problems Version 3.0, Part I – Theoretical Background, Part 2 – User's Manual," Sandia National Laboratories, SAND94-1173, SAND94-1179, Albuquerque, NM, 1998.

4. Summers, R. M., J. S. Peery, W. K. Wong, W. S. Hertel, T. G. Trucano and L. C. Chhabildas, "Recent progress in ALEGRA development and application to ballistic impacts," Sandia National Laboratories, SAND96-0045C, Albuquerque, NM, 1996.

5. McClaun, J. M., S. L. Thompson and M. G. Elrick, "CTH: A Three-Dimensional Shock Physics Code," *Int. J. Impact Engng*, vol. 10, pp. 351-360, 1990.

6. Schmitt, R. G., W. W. Erikson, A. I. Atwood and H. John, "Analysis of the NAWC Validation Cookoff Test," Proceedings of JANNAF 36th Combustion and 18th Propulsion Systems Hazards Subcommittee Meetings, Kennedy Space Center, FL, CPIA, 1999.

7. Atwood, A. I., P. O. Curran, D. M. Hanson-Parr, T. P. Parr and D. A. Ciaramitaro, "Experimental Input Parameters Required for Modeling the Response of PBXN-109 to Cookoff," Proceedings of JANNAF 37th Combustion and 19th Propulsion Systems Hazards Subcommittee Meetings, Monterey, CA, CPIA, 2000.

8. Erikson, W. W., R. G. Schmitt, A. I. Atwood and P. O. Curran, "Coupled Thermal-Chemical-Mechanical Modeling of Validation Cookoff Experiments," Proceedings of JANNAF 37th Combustion and 19th Propulsion Systems Hazards Subcommittee Meetings, Monterey, CA, 2000.

9. McClelland, M. A., T. D. Tran, B. J. Cunningham, R. K. Weese and J. L. Maienschein, "Cookoff Response of PBXN-109: Material Characterization and ALE3D Model," Proceedings of JANNAF 37th Combustion and 19th Propulsion Systems Hazards Subcommittee Meetings, Monterey, CA, CPIA, 2000.

10. McClelland, M. A., T. D. Tran, B. J. Cunningham, R. K. Weese and J. L. Maienschein, "Cookoff Response of PBXN-109: Material Characterization and ALE3D Thermal Predictions," Proceedings of 50th JANNAF Propulsion Meeting, Salt Lake City, UT, CPIA, 2001.

11. McClelland, M. A., J. L. Maienschein and A. L. Nichols, "Joint DoD/DOE Munitions Technology Development Program FY-01 Progress Report, Ignition and Initiation Phenomena: Cookoff Violence Prediction," Lawrence Livermore National Laboratory, 2002.

12. McGuire, R. R. and C. M. Tarver, "Chemical Decomposition Models for the Thermal Explosion of Confined HMX, TATB, RDX,and TNT Explosives," Proceedings of Seventh Symposium (International) on Detonation, Annapolis, MD, Naval Surface Weapons Center, 1981.

13. Steinberg, J., "Equation of State and Strength Properties of Selected Materials," Lawrence Livermore National Laboratories, UCRL-MA-106439, Livermore, CA, 1996.

14. Fried, L. E., W. M. Howard and P. C. Souers, "Cheetah 2.0 User's Manual," Lawrence Livermore National Laboratories, UCRL-MA-117541 Rev. 5, 1998.

15. Bird, R. B., W. E. Stewart and E. N. Lightfoot, *Transport Phenomena,* Wiley, pp. 260-261, 1960.

16. Catalano, E., R. McGuire, E. L. Lee, E. Wrenn, D. Ornellas and J. Walton, "The Thermal Decomposition and Reaction of Confined Explosives," Proceedings of Sixth International Symposium on Detonation, Coronado, CA, Office of Naval Research, 1976.

17. Nichols, A. L. and K. W. Westerberg, ""Modification of a Thermal Transport to Include Chemistry with Thermally Controlled Kinetics," *Numerical Heat Transfer, Part B*, vol. 24, pp. 489-503, 1993.

18. Shapiro, A. B. and E. A. L, "TOPAZ2D Heat Transfer Code Users Manual and Thermal Property Data Base," Lawrence Livermore National Laboratory, UCRL-ID-104558, 1990.

19. Avriel, M., *Nonlinear Programming: Analysis and Methods,* McGraw-Hill, pp. 4-1:4-20, 1970.

20. Maienschein, J. L. and J. B. Chandler, "Burn Rates of Pristine and Degraded Explosives at Elevated Pressures and Temperatures," Proceedings of 11th International Detonation Symposium, Snowmass, CO, Office of Naval Research, 1998.

21. Maienschein, J. L. and A. L. Nichols, "Joint DoD/DOE Munitions Technology Development Program FY-98 Progress Report, Ignition and Initiation Phenomena: Cookoff Violence Prediction," Lawrence Livermore National Laboratory, 1998.

22. Maienschein, J. L. and A. L. Nichols, "Joint DoD/DOE Munitions Technology Development Program FY-99 Progress Report, Ignition and Initiation Phenomena: Cookoff Violence Prediction," Lawrence Livermore National Laboratory, UCRL-ID-103482-98, 1999.

23. Atwood, A. I., personal communication, NAWC-CL, 2001.

24. Maienschein, J. L., A. L. Nichols and M. A. McClelland, "Joint DoD/DOE Munitions Technology Development Program FY-00 Progress Report, Ignition and Initiation Phenomena: Cookoff Violence Prediction," Lawrence Livermore National Laboratory, UCRL-ID-103482-00, 2001.

25. Morari, M. and E. Zafiriou, *Robust Process Control,* Prentice Hall, pp. 116-117, 1989.

26. Holman, J. P., *Heat Transfer,* McGraw-Hill, pp. 253-254, 1976.

27. Dube, E., R. Neely, A. L. Nichols, R. Sharp and R. Couch, "Users Manual for ALE3D An Arbitrary Lagrange/Eulerian 3D Code System," Lawrence Livermore National Laboratory, 2001.